

Earth and Space Science



RESEARCH ARTICLE

10.1029/2020EA001275

How to Recognize a True Mode of Atmospheric Circulation Variability

Radan Huth^{1,2}  and Romana Beranová²

¹Department of Physical Geography and Geoecology, Faculty of Science, Charles University, Prague, Czechia, ²Institute of Atmospheric Physics of the Czech Academy of Sciences, Prague, Czechia

Key Points:

- North Atlantic Oscillation, Arctic Oscillation, Barents Oscillation, and the summer East Atlantic pattern are examined as for their correspondence with underlying correlation structures and spatial and temporal subsampling
- Arctic Oscillation, Barents Oscillation, and the summer East Atlantic pattern are not true modes of atmospheric circulation variability
- We reiterate that rotated principal component analysis must be used to detect modes of circulation variability; the use of unrotated principal component analysis is more likely to result in statistical artifacts

Correspondence to:

R. Huth,
huth@ufa.cas.cz

Citation:

Huth, R. & Beranová, R. (2021). How to recognize a true mode of atmospheric circulation variability. *Earth and Space Science*, 8, e2020EA001275. <https://doi.org/10.1029/2020EA001275>

Received 11 AUG 2020
Accepted 29 JAN 2021

© 2021. The Authors.
This is an open access article under the terms of the [Creative Commons Attribution-NonCommercial License](https://creativecommons.org/licenses/by-nc/4.0/), which permits use, distribution and reproduction in any medium, provided the original work is properly cited and is not used for commercial purposes.

Abstract It has been demonstrated several times that when principal component analysis (PCA) is used for detection of modes of atmospheric circulation variability (teleconnections), principal components must be rotated. Despite it, unrotated PCA is still often used. Here we demonstrate on the examples of North Atlantic Oscillation (NAO), Arctic Oscillation (AO), Barents Oscillation (BO), and the summer East Atlantic (SEA) pattern that unrotated PCA results in patterns that are artifacts of the analysis method rather than true modes of variability. This claim is based on the comparison of the spatial patterns of the modes with spatial autocorrelations, on the sensitivity of the patterns to spatial and temporal subsampling, and, for the SEA pattern, on correlations with tropical sea surface temperature. Unlike NAO, which is defined by rotated PCA, the other modes, that is, AO, BO, and SEA pattern, defined by unrotated PCA, do not correspond well to underlying autocorrelation structures and are more sensitive to choices of spatial domain and time interval over which they are defined. We reiterate that a great care must be taken when interpreting outputs of PCA when applied to the detection of modes of circulation variability: a comparison with spatial autocorrelations and check for their spatial and temporal stability are necessary to distinguish true modes from statistical artifacts, which we call “ghost patterns.”

1. Introduction

Teleconnections are pairs (triples, quadruples, etc.) of geographically separated regions, which are highly correlated in geopotential heights, sea level pressure (SLP), or other atmospheric variables, whether positively or negatively. Their investigation dates back to the early twentieth century to studies by Walker and Bliss (1932) and Walker (1933) which were the first to introduce the notion of teleconnections into atmospheric sciences. Two major methods have been used to detect and describe teleconnections. One is based on autocorrelation maps (e.g., Handorf & Dethloff, 2009; Raible et al., 2014; Smoliak & Wallace, 2015; Wallace & Gutzler, 1981), which display correlations of a given reference point with all other points. To describe a complete autocorrelation structure of a SLP or height field, one would need a large pile of such maps, which makes their use impractical; Kousky and Bell (1992) may serve as a good example of such an attempt. Therefore, the other method, principal component analysis (PCA), gained much wider popularity. The pioneering studies to detect teleconnections by PCA, Barnston and Livezey (1987), Horel (1981), and Rogers (1981), demonstrated the suitability of PCA for this task; a few examples of recent studies using PCA include Gao et al. (2017), Lee et al. (2019), Liang et al. (2017), Lim (2015), and Mezzina et al. (2020). The association of outputs of PCA with physical processes is not straightforward (Spensberger et al., 2020). It should be noted that methods such as PCA “are not a priori constructed to extract information about dynamical behavior; they simply provide an efficient representation of variability” (Zwiers & von Storch, 2004). Such a representation of variability must, however, be in accord with what the first method of detection of teleconnections provides, that is, with the underlying autocorrelation structure (Richman, 1986).

PCA produces a series of principal components (PCs), each of which, in the setting used in this context (gridpoints in columns and time realizations in rows of the data matrix), that is, in an S-mode according to standard nomenclature (Richman, 1986), consists of three items: first, a pattern, commonly referred to as a “loading,” displays individual teleconnections as maps; it represents covariances or correlations of the PC with the original variables. Second, a corresponding time series, referred to as a “score” or “amplitude,” characterizes the intensity of each loading pattern at every time instant. And finally, an eigenvalue is a number that quantifies the variance accounted for by the PC. The terminology is not unified, however: within the empirical orthogonal function analysis framework (which is entirely equivalent to PCA), loadings are

often referred to as “empirical orthogonal functions” and scores as “principal components.” Outputs of PCA in the above setting applied to monthly or seasonal means, which this study deals with, are commonly referred to as “modes of low-frequency variability” (“modes of variability” in short).

PCs with close eigenvalues can blend with each other, which means that information they contain (i.e., variance they explain) can be mixed randomly, implying their interpretation may be misleading (North et al., 1982). A possible remedy to this degeneracy of eigenvalues is rotation of PCs (Jolliffe, 1989; Richman, 1986). Rotation is a linear transformation of PCs with the goal of approaching what is called “simple structure” or “sparse solution” as closely as possible. Simple structure (sparse solution) is characterized by component loadings attaining their values either near zero or near their possible maximum value (which is one if they represent correlations).

Another issue is the dependence of outputs of PCA on the shape and size of the domain on which the analysis is conducted. The structure of modes in unrotated PCA can result purely from the geometry of the domain, particularly if the autocorrelation distance of the variable analyzed and the size of the domain are comparable. A series of so-called Buell’s patterns with a predictable spatial structure, bearing resemblance to a harmonic decomposition, appears in such a case (Richman, 1993; Richman & Lamb, 1985). Buell’s patterns are not real representatives of underlying autocorrelation structure but statistical artifacts. They typically occur in unrotated solutions of PCA; rotation eliminates them quite effectively.

There are several criteria that may help in deciding whether the output of PCA is realistic and displays a true underlying autocorrelation structure or is rather an artifact of the method, which should not be interpreted. (1) Similarity with correlation/covariance maps. The real correlation/covariance structure of the analyzed field is described by its autocorrelation/autocovariance maps. Therefore, only those modes the loadings of which are similar to the autocorrelation/autocovariance maps can be considered as representing real correlation/covariance structures, that is, as true modes (e.g., Huth, 2006a; Lian & Chen, 2012; Richman & Lamb, 1985). (2) Insensitivity to spatial subsampling. The true teleconnections, corresponding to real autocorrelation structures, should appear as separate PCs regardless of the position and size of the domain on which PCA is conducted (provided that a sufficiently large area of the teleconnection is contained in the domain so that the signal of the teleconnection is strong enough not to be mistaken for noise) (e.g., Spensberger et al., 2020). (3) Insensitivity to temporal subsampling. Under the assumption of climate being stationary, the teleconnections should not change their structure and position considerably if different periods are used for the analysis (e.g., Cheng et al., 1995). Slight changes in the position and intensity of the action centers are, nevertheless, acceptable since they may indeed be reflections of real processes (Beranová & Huth 2007, 2008; Jung et al., 2003) or sampling uncertainty.

Several studies have unequivocally demonstrated that it is rotated PCA that must be used for detection of really occurring modes; when using unrotated PCA, one is at risk that statistical artifacts, including Buell’s patterns, rather than real modes are found (e.g., Compagnucci & Richman, 2008; Huth, 2006a; Kohyama & Hartmann, 2016; Lian & Chen, 2012; Richman & Lamb, 1985); also, unrotated modes are less robust against temporal and spatial subsampling (Cheng et al., 1995). In spite of this, unrotated PCA has been used to detect teleconnections in many studies. As a result, unrealistic patterns are interpreted as really occurring modes. We suggest to call such spurious, really nonexistent modes as “ghost patterns” simply because they share fundamental qualities with ghosts: Although they do not exist in reality, a number of people tend to believe in their existence and some people even believe they have seen them. One example of such ghost patterns are allegedly detected but unrealistic modes in sea surface temperature (Ashok et al., 2007; Zhang et al., 2010), disproved by Lian and Chen (2012).

Three striking examples of atmospheric structures that have been defined and identified by unrotated PCA are the subject of this study: Arctic Oscillation (AO), Barents Oscillation (BO), and summer East Atlantic (SEA) pattern. The AO was defined by Thompson and Wallace (1998) as the leading unrotated PC of 1,000 hPa heights, calculated from SLP by linear transformation, in the Northern Hemisphere Extratropics. Its physical realism has been questioned many times, mainly on the grounds of the lack of correlation between its centers (Ambaum et al., 2001; Deser, 2000; Huth, 2006b, 2007; Itoh, 2002); in spite of this, the concept of AO has been widely used until the present. The BO was defined as the second PC of SLP in winter over the Northern Extratropics north of 30°N (Skeie, 2000) or over the North Atlantic/European sector

Table 1
Principal Component Analysis Settings for the Detection of the Modes

	Months	Variable	Domain	Period	Rotation
NAO	November–March	SLP	North of 20°N	1948–2016	VARIMAX
AO	November–April	SLP	North of 20°N	1948–1997	None
BO	December–March	SLP	North of 30°N	1958–1999	None
SEA	June–August	500 hPa heights	40°N–70°N; 90°W–30°E	1979–2016	None

NAO, North Atlantic oscillation; SLP, sea level pressure; SEA, summer East Atlantic; AO, Arctic oscillation; BO, Barents oscillation.

(Chen et al., 2013). Its existence has been doubted by Tremblay (2001) by arguments similar to the concerns about the AO; in spite of that, Chen et al. (2013) elaborate the concept of BO further without attempting to cope with Tremblay (2001)'s criticism nor with general arguments against interpreting unrotated PCs. The SEA pattern was introduced by Wulff et al. (2017) who define it as the second PC of 500 hPa heights over the North Atlantic mid-latitudes in summer.

Our objective is to evaluate whether the AO, BO, and SEA are real teleconnection patterns by comparing them with autocorrelation maps and by evaluating their sensitivity to spatial and temporal subsampling. We contrast the behavior of the AO, BO, and SEA with the North Atlantic Oscillation (NAO), for the detection of which rotated PCA is routinely used. NAO is taken as a benchmark here because its realism is generally accepted and undoubted and physical processes governing it have been uncovered (e.g., Spensberger et al., 2020; Woolings et al., 2008).

2. Data and Methods

The data and settings of PCA are displayed in Table 1; they are selected so that they are as close as possible to those in the reference studies that introduced and described the AO, BO, and SEA, that is, in turn, Thompson and Wallace (1998), Skeie (2000), and Wulff et al. (2017). Monthly mean data from the NCEP/NCAR reanalysis (Kanamitsu et al., 2002) are used for all the analyses. NAO, AO, and BO are calculated from SLP for extended winter (November or December–March or April), while SEA is defined in 500 hPa heights in summer (June–August). Horizontal resolution of the data is 2.5° by 2.5°. The domain over which the NAO and AO are detected covers the Northern Hemisphere Extratropics north of 20°N inclusive. For BO, the analysis domain is the Northern Hemisphere north of 30°N inclusive. The SEA is detected on the regional window covering North Atlantic, Europe, and easternmost North America (40°–70°N, 90°W–30°E).

Covariance matrix is used as input to PCA. Data are weighted by square root of cosine of latitude to compensate for a decreasing area of gridboxes toward the pole. Unrotated PCA is used for the detection of AO, BO, and SEA, while NAO is detected by orthogonally rotated PCA (using the VARIMAX criterion) with nine modes retained. The retention and rotation of nine modes appears to be the best solution on the basis of the eigenvalue-PC number diagram (O'Lenic & Livezey, 1988) where the last drop occurs between the ninth and tenth PC and is in accord with hemispheric studies of teleconnections (e.g., Barnston & Livezey, 1987; Clinet & Martin, 1992; Huth et al., 2006; Hynčica & Huth, 2020).

We decided to compare PC loadings with autocorrelation maps, although PCA is based on the covariance matrix and autocovariance maps might seem more appropriate. The reason is that results do not differ between autocorrelation and autocovariance, and the interpretation of autocorrelation is more straightforward. Also, the arguments in previous studies that doubted the realism of the AO (Ambaum et al., 2001; Deser, 2000; Huth, 2006b, 2007; Itoh, 2002) are mostly based on (auto)correlations.

3. Description of Patterns

Patterns of all the four modes are displayed in Figure 1; their spatial structure is close to what is known from literature. NAO appears as a zonally oriented dipole with its southern center extending from central North Atlantic to southern Europe, the core of its northern center being located between Iceland and the southern

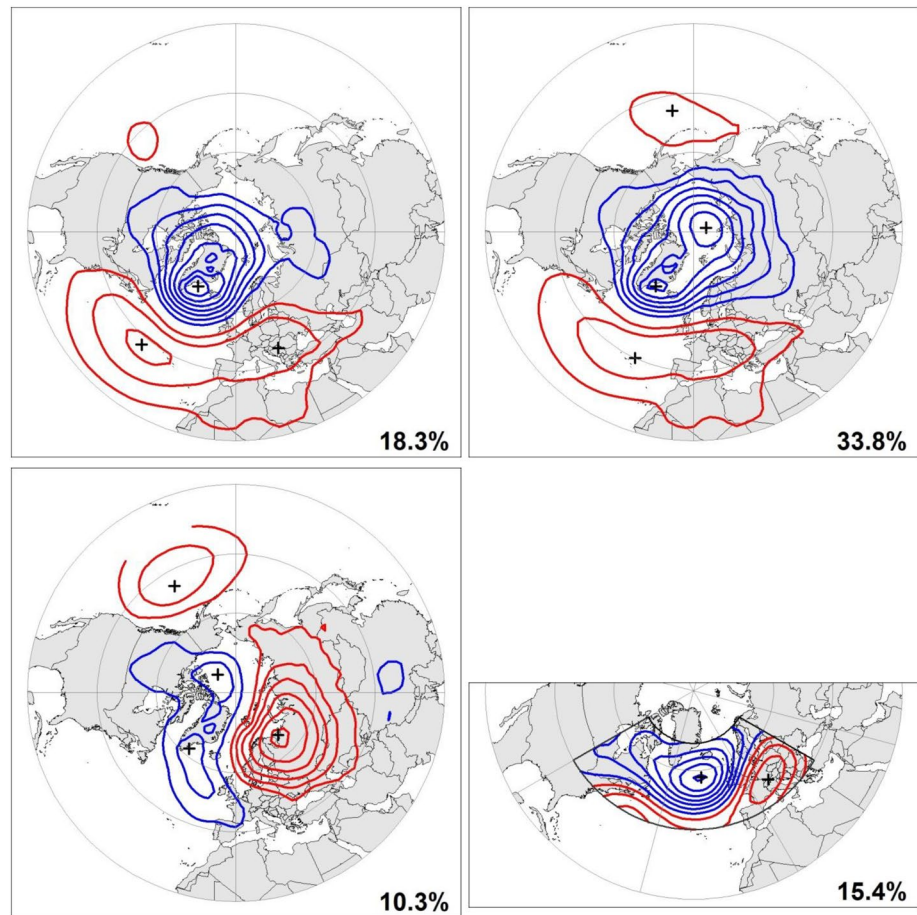


Figure 1. PC loading maps corresponding to North Atlantic Oscillation (a), Arctic Oscillation (b), Barents Oscillation (c), and summer East Atlantic pattern (d). For their definition see the text. Contour interval is 1 hPa in (a), (b), and (c); and 4 m in (d). Positive/negative contours are in red/blue, zero isoline is omitted. Crosses indicate points for which autocorrelation maps are displayed in Figures 2–5. For more details, see text. PC, principal component.

tip of Greenland. NAO is the second rotated PC and accounts for 18.3% of variance. This is considerably more than in other studies where NAO is defined by PCA of Northern Hemisphere Extratropics: about 12% in Barnston and Livezey (1987) and about 10% in Clinet and Martin (1992). This difference is likely to stem from the use of different data sources, variable (SLP here while mid-tropospheric heights in other studies), time period, the use of correlation or covariance matrix, and data processing.

AO explains 33.8% of total variance in the SLP data that we use. This is considerably more than 22%, reported by Thompson and Wallace (1998), but in a much better agreement with 36.8% reported by Skeie (2000). It is difficult to attribute the difference from Thompson and Wallace (1998) because the description of the methodology and settings of PCA is insufficient there for a full and successful replication (e.g., it is not clear how, and whether at all, the unequal grid size was compensated for and whether correlation or covariance matrix was used as an input). AO is a tripole, one of its centers residing over the Arctic, the other two centers of the opposite sign being located over the North Atlantic and southwestern Europe (in the area of the Azores high), and over the North Pacific (in the area of the Aleutian low). The Pacific center is considerably weaker in comparison with the other two centers and is somewhat weaker in our analysis than in Thompson and Wallace (1998).

BO explains 10.3% of total variance, ranking it as the second PC in terms of variance explained. It consists of a dipole with one center located over northern Eurasia and the other extending from west of the British Isles over Greenland and the Canadian Archipelago toward central Canada. An additional center is located

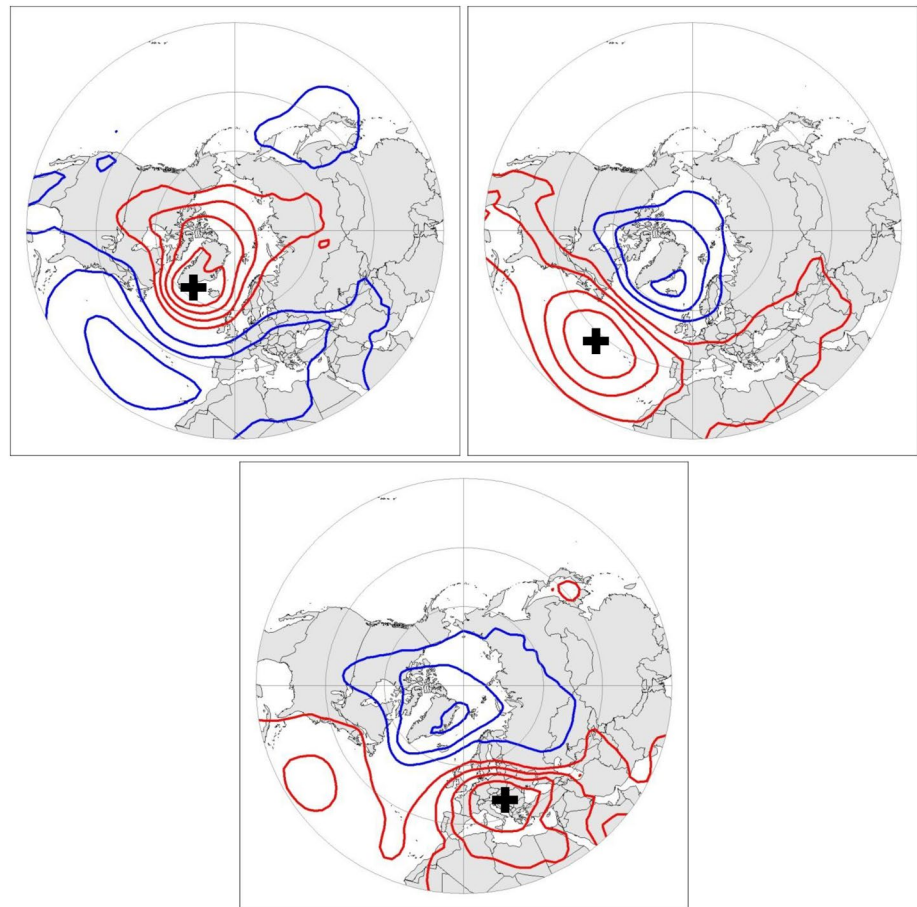


Figure 2. Autocorrelation maps for the centers of the NAO, indicated in Figure 1 by crosses. Contour interval is 0.2, positive/negative contours are in red/blue, zero isoline is omitted. The position of the reference point is indicated by a bold cross. NAO, North Atlantic Oscillation.

over eastern North Pacific along the 40°N parallel. Both the variance explained and the pattern agree well with Skeie (2000).

The SEA pattern forms a wavetrain-like structure with the main center northwest of the British Isles and secondary centers of opposite sign over central Europe and south of Newfoundland. SEA is the second mode in the Euro-Atlantic domain, explaining 15.4% of variance. There is a general correspondence with Wulff et al. (2017) both in terms of the variance explained (18%) and the spatial pattern; Wulff et al. (2017) localize the European center more northwards and the extension of the main center toward the U.S. is stronger there, however. The differences may be partly explained by the use of another reanalysis, namely ERA-Interim, by Wulff et al. (2017).

4. Correlation Structures

Let us start with the NAO. Figure 2 displays SLP autocorrelation maps for two points where PC loadings attain highest values of both signs: the core point of the Icelandic center (62.5°N, 35°W) and the core point of the Azores center (37.5°N, 40°W), and also for the point with the highest loading in the eastward extension of the Azores center toward southern Europe (45°N, 20°E). The Icelandic center (Figure 2 top left) is strongly correlated with the entire belt along the 40°N parallel, which forms the Azores center. The autocorrelation with the Azores center (Figure 2 top right) bears also a strong resemblance to the NAO pattern as produced by rotated PCA. The correlation with its eastward extension is weaker than what the NAO pattern suggests; the interpretation of this fact is that the western and eastern parts of the Azores center

Table 2

Pattern Correlations Between the Spatial Patterns of the Modes and Autocorrelation Maps for the Central Points (Identified by Latitude/Longitude) of Their Action Centers, Calculated Over the Domains on Which the Modes are Defined

Mode	NAO		AO		BO		SEA	
	62.5°N/35°W	0.95	40°N/25°W	0.81	70°N/45°E	0.54	55°N/25°W	-0.77
	37.5°N/40°W	-0.86	65°N/35°W	-0.90	62.5°N/40°W	-0.29	47.5°N/10°E	0.89
	45°N/20°E	-0.82	85°N/110°E	-0.97	80°N/135°W	-0.42		
			45°N/170°W	0.36	45°N/150°W	0.41		

NAO, North Atlantic oscillation; AO, Arctic oscillation; SEA, summer East Atlantic; BO, Barents oscillation.

strongly correlate with the Icelandic center, but their mutual correlation is weaker, which is confirmed by the autocorrelations with the eastern part of the Azores center (Figure 2 bottom). All in all, the autocorrelation structures correspond to the rotated PC loadings forming NAO (Figure 1), which is also demonstrated by the pattern correlations between the NAO pattern and the three autocorrelation maps all exceeding 0.8 (Table 2). We can claim, therefore, that the NAO produced by rotated PCA reflects its underlying autocorrelation structure and is a realistic representation of SLP variability.

Autocorrelation maps for the AO are displayed in Figure 3 for the core points of its three centers (that is, the points with the highest loadings of either sign; 40°N, 25°W for the Atlantic center; 65°N, 35°W and 85°N,

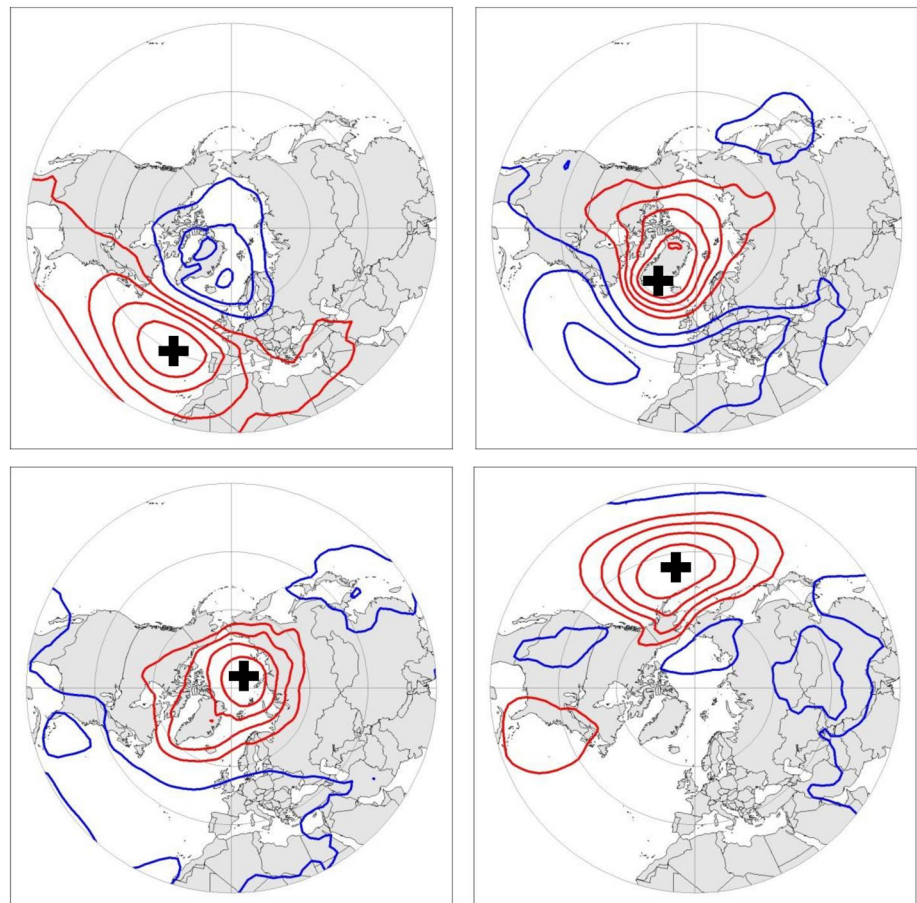


Figure 3. As in Figure 2, but for the AO. AO, Arctic Oscillation.

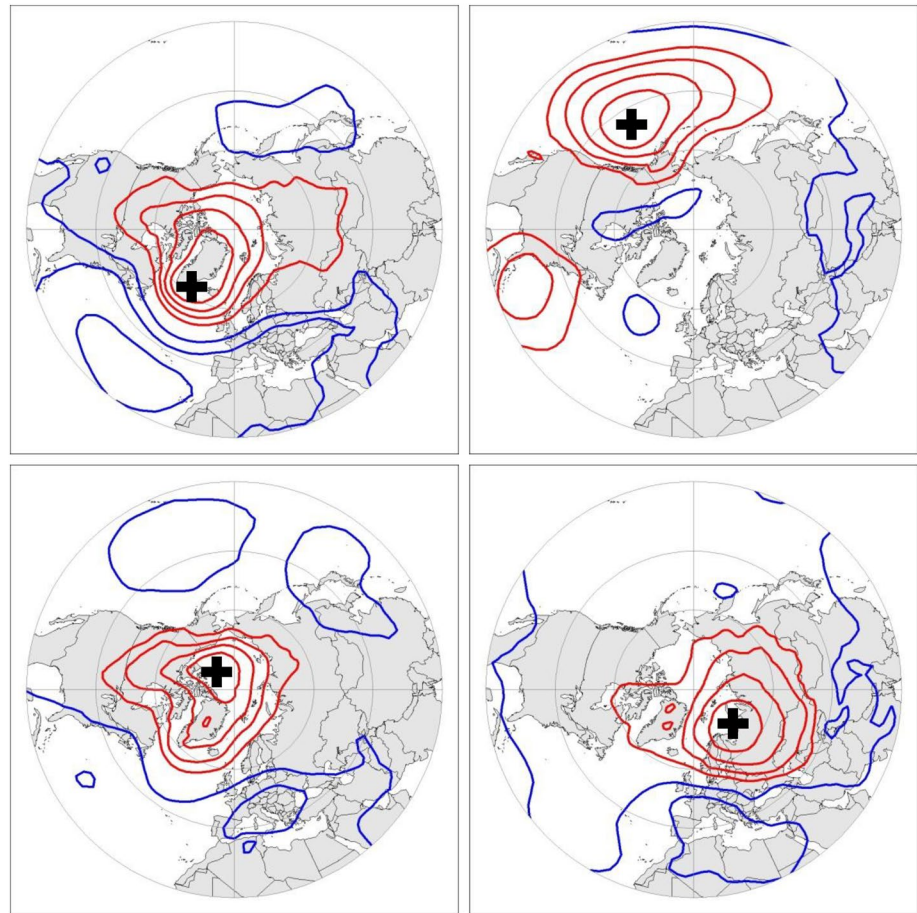


Figure 4. As in Figure 2, but for the BO. BO, Barents Oscillation.

110°E for two cores of the Arctic center; and 45°N, 170°W for the Pacific center). Since the core point of the Azores center of the AO is close to the center of the NAO, it is natural and expectable that the corresponding autocorrelation map resembles that for the NAO. There are clearly no hints of the Aleutian center there. The correlation maps for the two cores of the Arctic center differ considerably, pointing to the lack of coherence between them, namely, between the northern North Atlantic and the area north of the Siberian coast. The map for the former closely resembles the NAO; note that the area of weak negative correlations centered over northern Japan is far away from the area where the Aleutian center occurs and is unrelated to it. The map for the latter exhibits only weak correlations with the mid-latitude belt over the North Atlantic and there is no link to the Aleutian center either. The Aleutian center is not correlated with the Azores center at all; the correlations are below 0.2, which indicates they are not different from zero at the 5% significance level according to *t*-test (the critical value under the assumption of temporal independence is 0.24). No correlations of the Aleutian center are detected with the Arctic center either, with the exception of a tiny area over the East Siberian Sea. Pattern correlation of the correlation map with the AO pattern is 0.36 only (Table 2). In fact, the autocorrelation map of the Aleutian center is reminiscent of the second rotated PC of SLP in the Northern Hemisphere and the first PC in the Pacific domain, which corresponds to a manifestation of the Pacific-North American pattern in SLP (e.g., Linkin & Nigam, 2008; Yeh et al., 2018). Our results clearly confirm that there is no linear link between the Aleutian center of the AO and its other two centers. The AO does not correspond to the underlying autocorrelation structure.

Figure 4 shows autocorrelation maps for the BO, namely for two cores of its negative center, one near the southern tip of Greenland and the other northwest of the Canadian Archipelago (62.5°N, 40°W and 80°N, 135°W), the Siberian center (70°N, 45°E), and the secondary center over the eastern North Pacific (45°N, 150°W). What all of them display is entirely dissimilar from the pattern of the BO as shown in Figure 1:

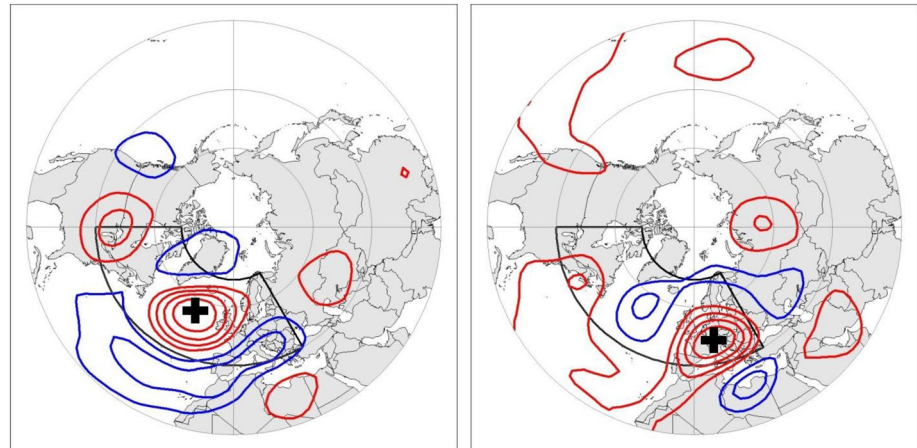


Figure 5. As in Figure 2, but for the SEA pattern. Bold black lines delineate the domain on which the pattern is defined. SEA, summer East Atlantic.

there is no indication in the autocorrelation maps of a dipole with the zero line from the British Isles through the central Arctic to eastern Siberia. Instead of it, one can see a NAO-like pattern in correlations with the Greenland center and a rather weak but spatially extensive dipole in correlations with the Siberian center. There is no correlation between the Pacific center with the rest of the BO pattern, indicating that its attachment to the BO pattern is an artifact of unrotated PCA. The autocorrelation maps together with low pattern correlations in Table 2 demonstrate clearly that the centers of BO do not correlate at all. BO does not correspond to a real autocorrelation structure either.

Autocorrelation maps of the two major centers of the SEA pattern (55°N , 25°W over the North Atlantic and 47.5°N , 10°E over central Europe; Figure 5) share the basic feature of the loading map consisting of a dipole between the North Atlantic southwest of Iceland and the Alps. However, a substantial difference appears in the western part of the domain over eastern Canada: instead of being strongly correlated with the Atlantic center, as suggested by the loading, it is weakly correlated with the Alpine center. The correlations in Table 2 are not as low as for AO and BO; this is probably because the PC loading and corresponding autocorrelation maps only differ over a minor part of the domain, although substantially. In summary, neither the SEA pattern does reflect the autocorrelation structure.

5. Spatial Subsampling

As already mentioned in the Introduction, real modes should have the same appearance regardless of how the analysis domain is positioned, provided that large enough part of the mode is covered by the domain so that the signal related to it is strong enough to be detectable. We perform three sets of experiments to test the sensitivity of spatial patterns of NAO, AO, and BO to the analysis domain. First, the hemispheric analysis domain is contracted from the south with the step of 10° ; that is, the domains on which the modes are identified are 20°N to the pole (standard for NAO and AO), 30°N to the pole (standard for BO), 40°N to the pole, etc. Second, the domain is contracted from the north with the same step; that is, the domains are 20° – 80°N , 20° – 70°N , etc. Finally, the analyses are conducted on halves of the full domain, that is, on 180° wide sectors, with the step of 45° of longitude. These domains are limited from the south by the 20°N parallel on one hand and by 0° and 180° , 45°E and 135°W , etc., on the other; eight such sectors are formed altogether.

Figure 6 demonstrates that the spatial structure of NAO changes only a little when it is defined on various spatial domains. It is almost insensitive to changes in the southern boundary of the domain. The similarity of the pattern with full NAO is very high even with the southern boundary at 50°N , which means that the almost entire southern center is left out, remaining outside the domain, so that it cannot have any effect on the shape of the loading pattern. When NAO is analyzed on a latitudinal belt, the similarity with full NAO remains high until the northern boundary moves to 70°N (not shown). When only the domain between 20° and 60°N is analyzed, NAO splits into two modes, which separate its southern center into a western

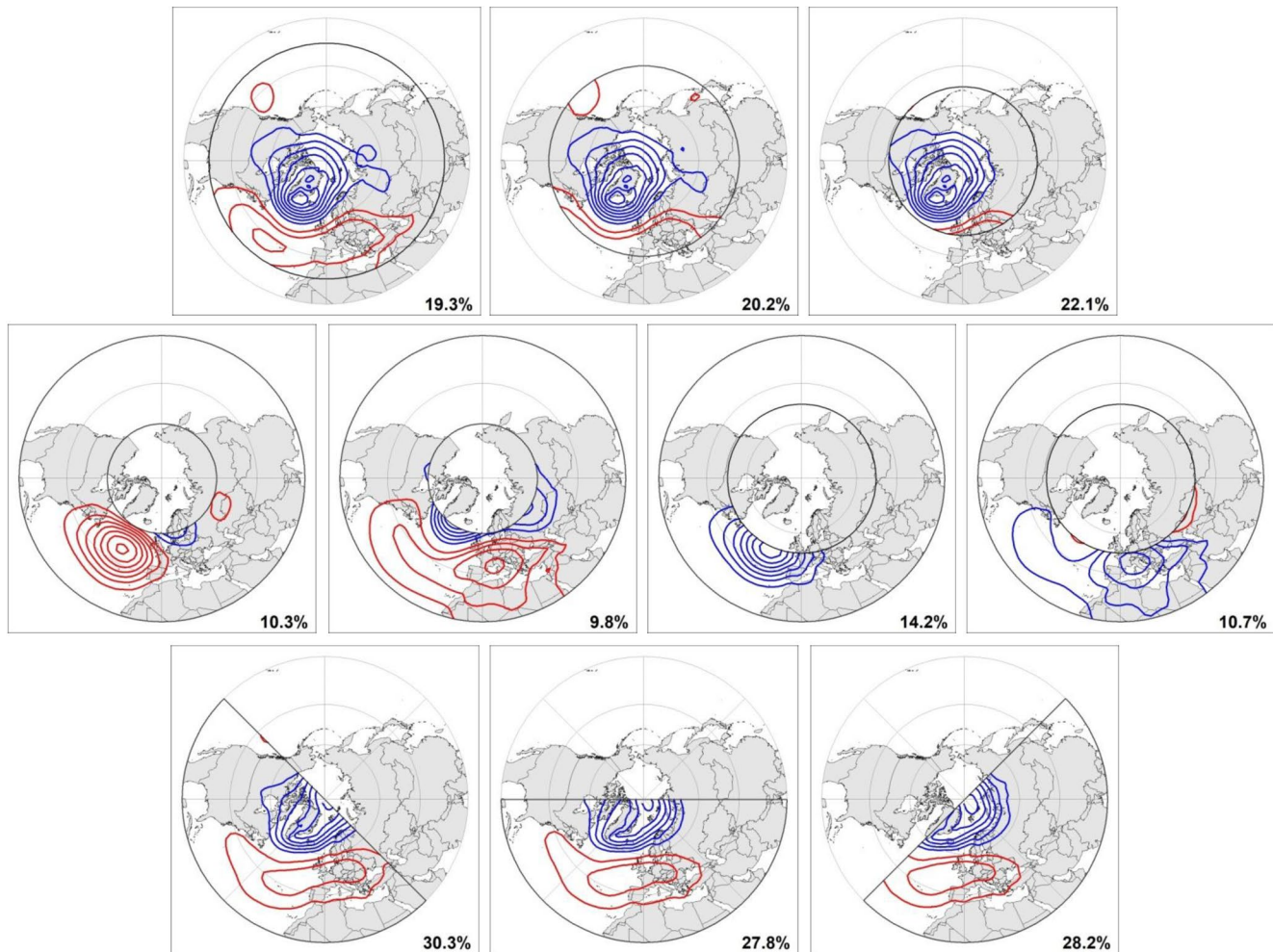


Figure 6. PC loading maps for NAO defined on subdomains; displayed as in Figure 1. Upper row from left: north of 30°N, north of 40°N, and north of 50°N, all PC 1. Middle row: PC 2 of 20°–60°N, PC 3 of 20°–60°N, PC 2 of 20°–50°N, and PC 3 of 20°–50°N. Bottom row: 135°W to 45°E, 90°W to 90°E, and 45°W to 135°E, all north of 20°N and PC 1. NAO, North Atlantic Oscillation; PC, principal component.

(Atlantic) and eastern (European) part. This is a consequence of the northern center being not considered in the analysis: Since two parts of the southern center are jointed weakly and are kept together thanks to their strong link with the northern center (as autocorrelation maps in Figure 2 suggest), the two parts split apart when their bonds to the northern center are excluded from the analysis. It should be noted; however, that despite the split, the two new modes bear a considerable similarity to full NAO. When the domain is reduced further to 20°–50°N, the two modes display little change, their similarity to the two parts of full NAO being retained. If only 180° wide sectors are analyzed, the patterns also remain strongly similar to full NAO.

AO is not sensitive to the contraction of the analysis domain from south (Figure 7), nor is it sensitive to changes in the northern boundary up to 70°N (not shown). Similarly to NAO, AO splits into two modes for the domain 20°–60°N; the substantial difference is, however, that the similarity of the mode corresponding to the Aleutian center with full AO is small: the center is differently shaped and much stronger. The Aleutian and Atlantic center with magnitudes corresponding to the full AO pattern appear together in one mode (PC 3) in the narrower belt from 20° to 50°N; however, their signs are opposite, which contradicts the pattern of full AO where the two centers have the same sign. Patterns obtained in the 180° wide sectors are similar to full AO (not shown).

Also BO is fairly stable if the analysis domain is contracted from south (Figure 8). The two major centers are retained even if the domain is reduced from north; the Siberian center, however, moves southward with the

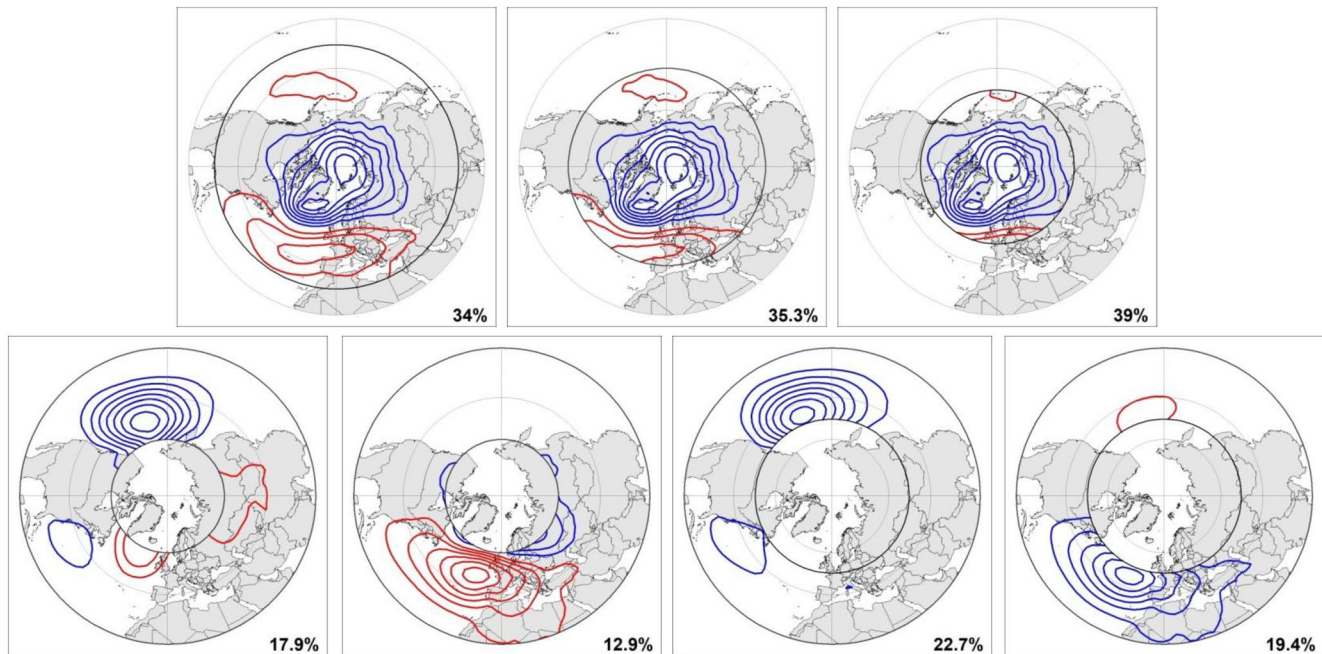


Figure 7. PC loading maps for AO defined on subdomains; displayed as in Figure 1. Upper row from left: north of 30°N, north of 40°N, and north of 50°N, all PC 1. Bottom row: PC 1 of 20°–60°N, PC 2 of 20°–60°N, PC 1 of 20°–50°N, and PC 2 of 20°–50°N. AO, Arctic Oscillation; PC, principal component.

shift of the northern edge of the domain: while it is near 70°N for the full domain, it is at or even slightly south of 60°N for the 20°–60°N domain. The other, and more substantial, difference between full BO and the modes on the annular domains is the appearance of a new center over the Atlantic: while only a very small and weak hint of a center can be seen west of the Azores for the full domain, a large and strong center straddling the Atlantic Ocean appears for the domain bounded by 60°N. There is no support for such a center in autocorrelation maps: the correlation between the two centers with high positive loadings is near zero and insignificant. Even more considerable differences in BO can be seen between the full domain and the longitudinal sectors. Over some sectors (e.g., between 180° and 0° over North America), no mode even marginally similar to BO appears. For the sectors where modes resembling BO can be found, the differences from full BO are substantial.

The spatial (in)stability of the SEA mode is demonstrated for domains shifted longitudinally. Figure 9 shows the modes corresponding to SEA for domains shifted by 30° west and east relative to the original domain. The modes in different domains are similar to each other in that the more or less circular major center over the central North Atlantic is flanked by more elongated centers of the opposite sign. However, a closer look reveals that the position of the centers differs: the major center for the domain shifted west (120°W–0°E) is located southwestward of its position in the “standard” domain, whereas the major center for the domain shifted east (60°W–60°E) is located southeastward of it. The position and shapes of the other two centers differ between the domains considerably as well.

6. Temporal Subsampling

The sensitivity to temporal subsampling is examined by comparing the modes calculated for three subsets containing every third year, each composed of 23 years: the first subset contains years 1948, 1951, 1954, ..., 2014, the second one contains years 1949, 1952, ..., 2015, and the third one contains years 1950, 1953, ..., 2016. This composition of subsets has the advantage that possible long-term variability and trends need not be considered in the interpretation of results. Whereas NAO does not almost change its shapes from one subset to another (not shown), the modes defined by unrotated PCA are considerably less temporally stable (Figure 10). This is in line with North et al. (1982)'s estimates of uncertainty in the determination of PCs:

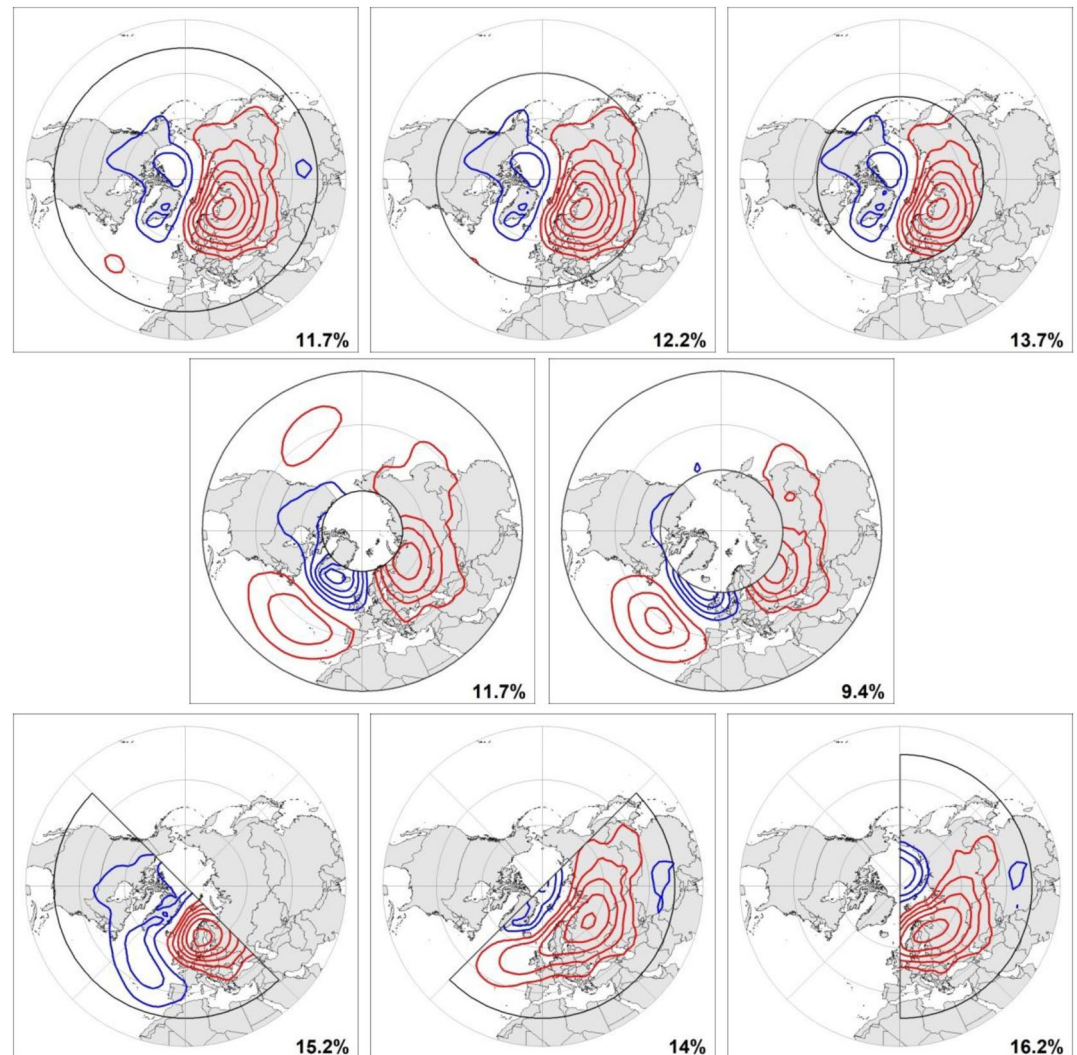


Figure 8. PC loading maps for BO defined on subdomains; displayed as in Figure 1. Upper row from left: north of 30°N, north of 40°N, and north of 50°N, all PC 2. Middle row: PC 3 of 20°–70°N and PC 4 of 20°–60°N. Bottom row: 135°W–45°E, 45°W–135°E, and 0°–180°, all north of 20°N and PC 2. BO, Barents Oscillation; PC, principal component.

The error bars around eigenvalues grow when sample size decreases, leading to a higher chance of overlap between them, which indicates potential for blending unrotated PCs together.

The Pacific center of the AO varies its position both latitudinally (from 40° N to 50° N) and longitudinally. The prominence of its Arctic center along 70°E changes its latitudinal extension by about 15°, and so does its Atlantic center over Africa. BO is highly sensitive to the choice of data subset, which manifests in

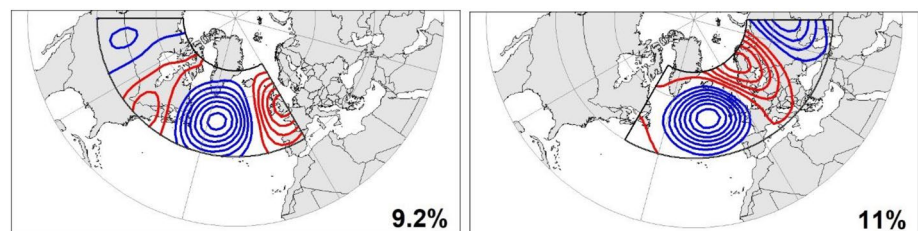


Figure 9. PC loadings corresponding to SEA for shifted domains; displayed as in Figure 1: 40°–70°N, 120°W–0°E (left); 40°–70°N, 60°W–60°E (right). SEA, summer East Atlantic; PC, principal component.

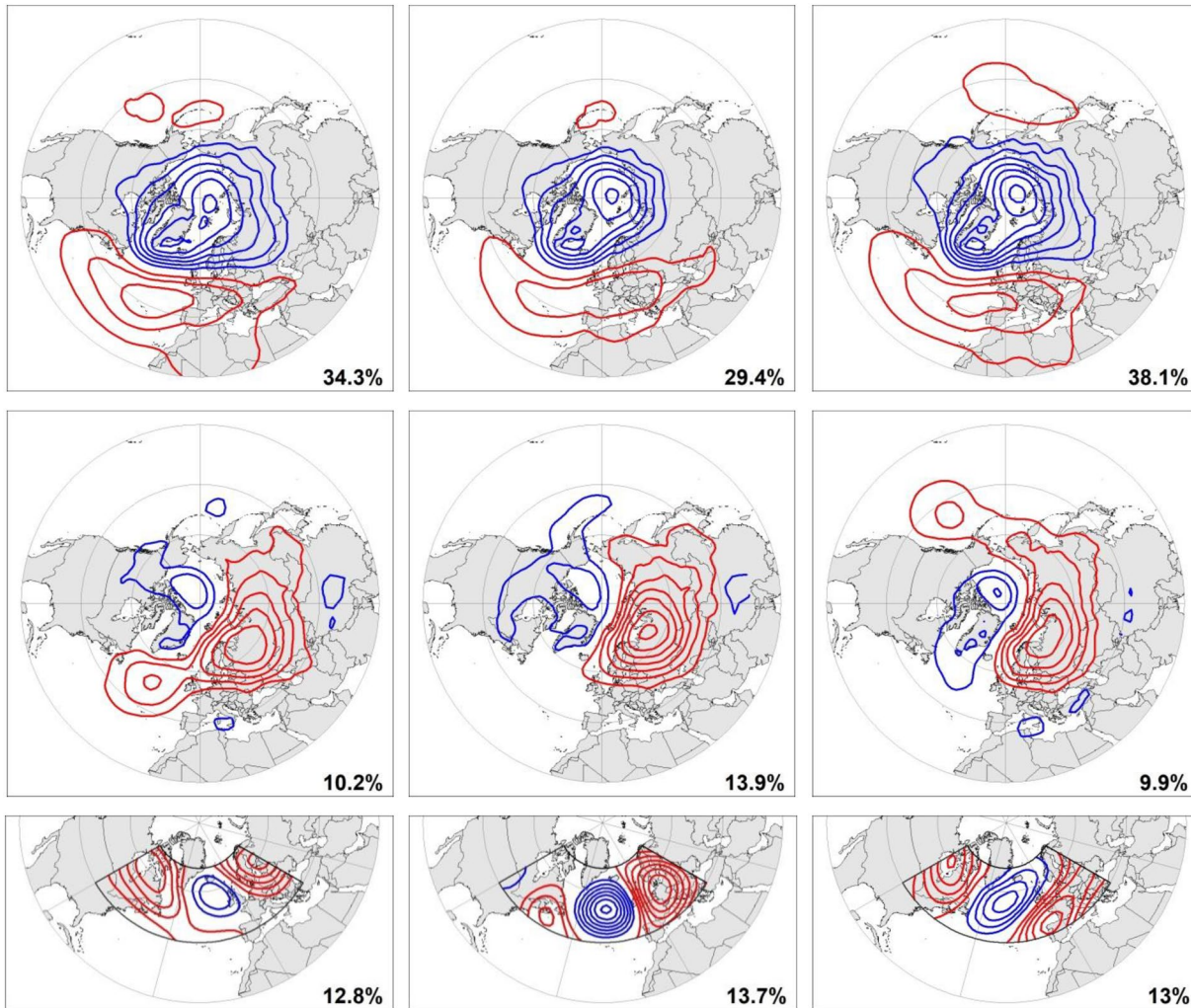


Figure 10. PC loadings for (from top to bottom) AO, BO, and SEA mode in datasets consisting of every third year, starting from (from left to right) 1948, 1949, and 1950; PC 1 in all datasets for AO, PC 3 in the data set starting from 1948 and PC 2 in the other datasets for BO, PC 3 in all datasets for SEA mode. SEA, summer East Atlantic; PC, principal component; BO, Barents Oscillation; AO, Arctic Oscillation.

changing extensions of the Siberian center into the North Atlantic and northeast Pacific and in varying size of the Canadian center. We note that although Chen et al. (2013) report a substantial disagreement in the spatial structure of BO between different periods (1949–1976 and 1977–2011), they do not consider such a temporal instability as a signature of the lack of realism of BO.

Similar to BO, the mode corresponding to the SEA pattern differs in its shapes between the three subsets. While the SEA pattern always appears as a tripole, the position of its centers and orientation of gradients between them is different.

7. Further Arguments Related to SEA

One of the arguments Wulff et al. (2017) use to support the existence of the SEA pattern is its correlations with surface temperature in the Tropical Pacific and Caribbean Basin, suggesting a tropical origin of its forcing. Here we demonstrate that any extratropical pattern, regardless of whether it is a variability mode or not, may be remotely correlated with tropical temperature. To this end, we form two extratropical patterns that are not modes of variability because they are not obtained by PCA, by simply shifting the SEA pattern by 30° to the east and then 20° to the south (left column in Figure 11), and calculate their correlations with surface temperature (right column in Figure 11). Obviously, not only the true SEA mode, but also the

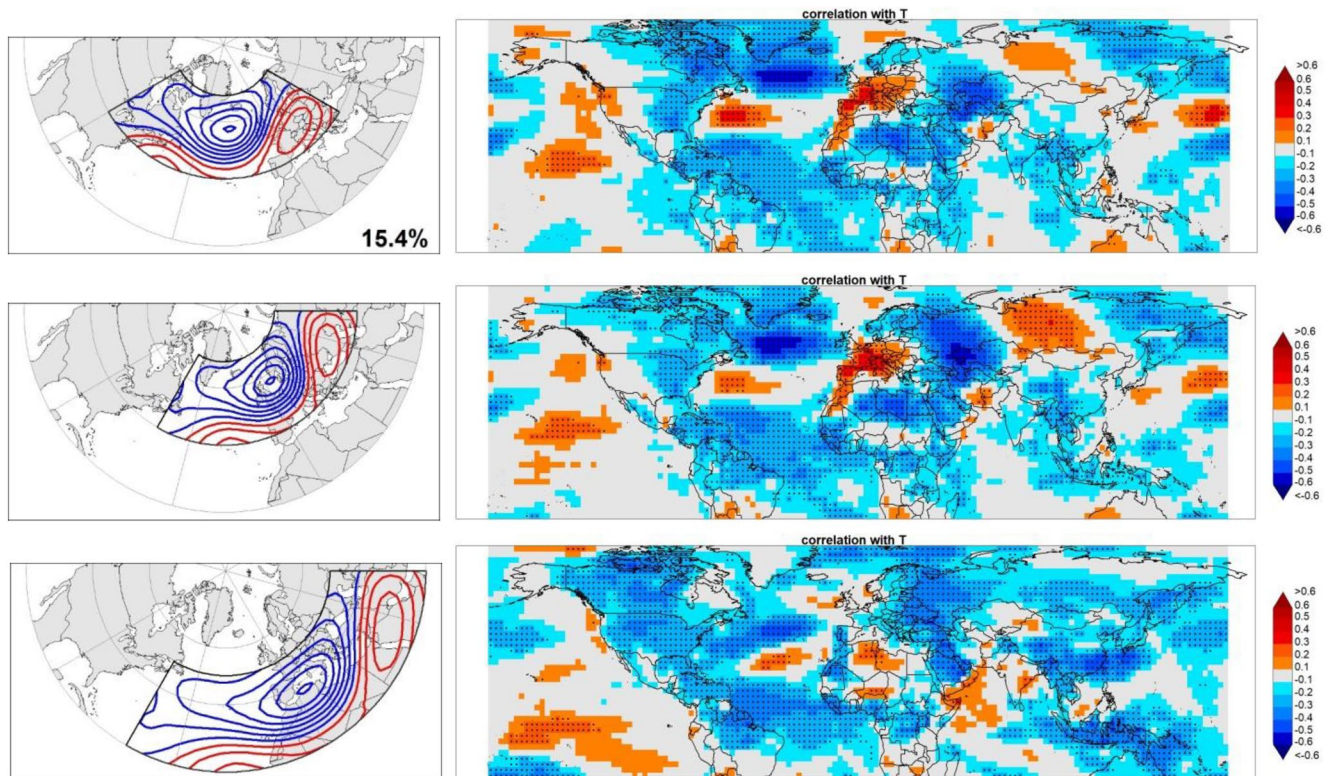


Figure 11. Left column, from top: original SEA pattern detected by principal component analysis as in Figure 1, SEA pattern shifted 30° east, and SEA pattern shifted 30° east and 20° south. Right column: correlations of the patterns in the left column with surface temperature. Black dots denote statistical significance at the 5% level. SEA, summer East Atlantic.

shifted patterns are significantly correlated with temperature in the Tropical Pacific, Caribbean, and even in the tropical Indian Ocean. This demonstrates that the existence of remote correlations, possibly implying remote forcing, does not provide support to the realism of a mode.

8. Conclusions

Four modes of variability, NAO, AO, BO, and the SEA pattern, are examined as to whether they can be considered real modes of variability or artifacts of the analysis method. Whereas NAO is detected by rotated PCA, unrotated PCA is used for the detection of the other modes, in line with their conventional definition. The realism of the modes is assessed by four tools. First, the loading maps, representing spatial structure of the modes, are compared with autocorrelation maps, displaying real correlation structures, which PCA and the modes are expected to describe. Second, the sensitivity to spatial subsampling is evaluated by calculating PCA on various subdomains. Third, the sensitivity to temporal subsampling is estimated by separate analyses of three data subsets, each being composed of every third year. And finally, the correlations with temperature in the Tropics are examined for the SEA mode and compared with patterns, obtained by a longitudinal and latitudinal translation of the SEA mode, which have no support in PCA.

All the analyses indicate that unlike NAO, which is a really occurring mode of circulation variability, closely resembling the underlying correlation structure and exhibiting a fairly little sensitivity to spatial and temporal subsampling, AO, BO, and SEA mode should be viewed of as artifacts of the analysis method, for which we introduce term “ghost patterns”: although such patterns, similarly to ghosts, do not exist in reality, many people believe in their existence and even believe they have seen them. AO, BO, and SEA mode exhibit, although to a different extent, the lack of similarity of their spatial representation with autocorrelation maps and the lack of stability when the analysis domain and period are altered. The weakest part of AO is

its Pacific center, which is uncorrelated with the other two centers (Arctic and Atlantic) and its appearance and even its presence are sensitive to the choice of the domain and analysis period.

Our results support the outcomes of previous studies (e.g., Ambaum et al., 2001; Deser, 2000; Huth, 2006b, 2007; Itoh, 2002), which were mostly based on autocorrelation maps and focused on AO only, and extend them by additional arguments, following from the spatial and temporal stability of the modes, and to other alleged modes introduced into scientific literature in the past 20 years, viz., BO and SEA pattern. Our results have also implications for comparisons of atmospheric circulation between different datasets, for example, among reanalyses or between climate models and reality. It makes sense to conduct such comparisons for real modes only; there is no reason to penalize a particular data set (reanalysis, climate model) for not being able to reproduce a ghost pattern, that is, an artifact of an analysis method that is not real.

One must be very careful when interpreting outputs of PCA. A check of the resultant patterns against autocorrelation structure and a test of their stability against spatial and temporal subsampling are necessary before the pattern identified by PCA can be claimed to be a physically realistic mode. There is a high risk that unrotated PCA may provide artifacts instead of real modes of variability; the use of rotated PCA is highly recommended to avoid identification of spurious ghost patterns.

Conflicts of Interest

The authors declare no conflicts of interest relevant to this study.

Data Availability Statement

Publicly available data (NCEP/NCAR reanalysis) were only used.

Acknowledgments

The NCEP/NCAR reanalysis was downloaded from <https://psl.noaa.gov/data/gridded/data.ncep.reanalysis.html>. This study was funded by the Czech Science Foundation, project 17-07043S.

References

- Ambaum, M. H. P., Hoskins, B. J., & Stephenson, D. B. (2001). Arctic oscillation or North Atlantic oscillation? *Journal of Climate*, *14*, 3495–3507.
- Ashok, K., Behera, S. K., Rao, S. A., Weng, H., & Yamagata, T. (2007). El Niño Modoki and its possible teleconnection. *Journal of Geophysical Research*, *112*, C11007. <https://doi.org/10.1029/2006JC003798>
- Barnston, A. G., & Livezey, R. E. (1987). Classification, seasonality and persistence of low-frequency atmospheric circulation patterns. *Monthly Weather Review*, *115*, 1083–1126.
- Beranová, R., & Huth, R. (2007). Time variations of the relationships between the North Atlantic oscillation and European winter temperature and precipitation. *Studia Geophysica et Geodaetica*, *51*, 575–590.
- Beranová, R., & Huth, R. (2008). Time variations of the effects of circulation variability modes on European temperature and precipitation in winter. *International Journal of Climatology*, *28*, 139–158. <https://doi.org/10.1002/joc.1516>
- Cheng, X., Nitsche, G., & Wallace, J. M. (1995). Robustness of low-frequency circulation patterns derived from EOF and rotated EOF analyses. *Journal of Climate*, *8*, 1709–1713.
- Chen, H. W., Zhang, Q., Körnisch, H., & Chen, D. (2013). A robust mode of climate variability in the Arctic: The Barents oscillation. *Geophysical Research Letters*, *40*, 2856–2861. <https://doi.org/10.1002/grl.50551>
- Clinet, S., & Martin, S. (1992). 700-hPa geopotential height anomalies from a statistical analysis of the French Hemis data set. *International Journal of Climatology*, *12*, 229–256.
- Compagnucci, R. H., & Richman, M. B. (2008). Can principal component analysis provide atmospheric circulation or teleconnection patterns? *International Journal of Climatology*, *28*, 703–726. <https://doi.org/10.1002/joc.1574>
- Deser, C. (2000). On the teleconnectivity of the “Arctic oscillation”. *Geophysical Research Letters*, *27*, 779–782. <https://doi.org/10.1029/1999GL010945>
- Gao, T., Yu, J. Y., & Paek, H. (2017). Impacts of four northern-hemisphere teleconnection patterns on atmospheric circulations over Eurasia and the Pacific. *Theoretical and Applied Climatology*, *129*, 815–831. <https://doi.org/10.1007/s00704-016-1801-2>
- Handorf, D., & Dethloff, K. (2009). Atmospheric teleconnections and flow regimes under future climate projections. *The European Physical Journal – Special Topics*, *174*, 237–255. <https://doi.org/10.1140/epjst/e2009-01104-9>
- Horel, J. D. (1981). A rotated principal component analysis of the interannual variability of Northern Hemisphere 500 mb height field. *Monthly Weather Review*, *109*, 2080–2092.
- Huth, R. (2006a). The effect of various methodological options on the detection of leading modes of sea level pressure variability. *Tellus A*, *58*, 121–130. <https://doi.org/10.1111/j.1600-0870.2006.00158.x>
- Huth, R. (2006b). Pacific center of the Arctic oscillation: Product of high local variability rather than teleconnectivity. *Tellus A*, *58*, 601–604. <https://doi.org/10.1111/j.1600-0870.2006.00203.x>
- Huth, R. (2007). Arctic or North Atlantic oscillation? Arguments based on the principal component analysis methodology. *Theoretical and Applied Climatology*, *89*, 1–8. <https://doi.org/10.1007/s00704-006-0257-1>
- Huth, R., Pokorná, L., Bochniček, J., & Hejda, P. (2006). Solar cycle effects on modes of low-frequency circulation variability. *Journal of Geophysical Research*, *111*, D22107. <https://doi.org/10.1029/2005JD006813>
- Hynčica, M., & Huth, R. (2020). Modes of atmospheric circulation variability in the Northern Hemisphere: A comparison of five reanalyses. *Journal of Climate*, *33*, 10707–10726. <https://doi.org/10.1175/JCLI-D-19-0904.1>

- Itoh, H. (2002). True versus apparent Arctic oscillation. *Geophysical Research Letters*, 29, 109. <https://doi.org/10.1029/2001GL013978>
- Jolliffe, I. T. (1989). Rotation of ill-defined principal components. *Applied Statistics*, 38, 139–147.
- Jung, T., Hilmer, M., Ruprecht, E., Kleppek, S., Gulev, S. K., & Zolina, O. (2003). Characteristics of the recent eastward shift of interannual NAO variability. *Journal of Climate*, 16, 3371–3382.
- Kanamitsu, M., Ebisuzaki, W., Woollen, J., Yang, S.-K., Hnilo, J. J., Fiorino, M., & Potter, G. L. (2002). NCEP-DOE AMIP-II reanalysis (R-2). *Bulletin of the American Meteorological Society*, 83, 1631–1643.
- Kohyama, T., & Hartmann, D. L. (2016). Antarctic sea ice response to weather and climate modes of variability. *Journal of Climate*, 29, 721–741. <https://doi.org/10.1175/JCLI-D-15-0301.1>
- Kousky, V. E., & Bell, G. D. (1992). Atlas of Southern Hemisphere 500 mb teleconnection patterns derived from national meteorological center analyses. *NOAA Atlas*, 9, 1–90.
- Lee, J. W., Sperber, K. R., Gleckler, P. J., Bonfils, C. J. W., & Taylor, K. E. (2019). Quantifying the agreement between observed and simulated extratropical modes of interannual variability. *Climate Dynamics*, 52, 4057–4089. <https://doi.org/10.1007/s00382-018-4355-4>
- Liang, Y.-C., Yu, J.-Y., Saltzman, E. S., & Wang, F. (2017). Linking the tropical Northern Hemisphere pattern to the Pacific warm blob and Atlantic cold blob. *Journal of Climate*, 30, 9041–9057. <https://doi.org/10.1175/JCLI-D-17-0149.1>
- Lian, T., & Chen, D. (2012). An evaluation of rotated EOF analysis and its application to Tropical Pacific SST variability. *Journal of Climate*, 25, 5361–5373. <https://doi.org/10.1175/JCLI-D-11-00663.1>
- Lim, Y.-K. (2015). The East Atlantic/West Russia (EA/WR) teleconnection in the North-Atlantic: Climate impact and relation to Rossby wave propagation. *Climate Dynamics*, 44, 3211–3222. <https://doi.org/10.1007/s00382-014-2381-4>
- Linkin, M. E., & Nigam, S. (2008). The North Pacific Oscillation-West Pacific teleconnection pattern: Mature-phase structure and winter impacts. *Journal of Climate*, 21, 1979–1997. <https://doi.org/10.1175/2007JCLI2048.1>
- Mezzina, B., Garcia-Serrano, J., Blade, I., & Kucharski, F. (2020). Dynamics of the ENSO teleconnection and NAO variability in the North Atlantic-European late winter. *Journal of Climate*, 33, 907–923. <https://doi.org/10.1175/JCLI-D-19-0192.1>
- North, G. R., Bell, T. C., Cahalan, R. F., & Moeng, F. J. (1982). Sampling errors in the estimation of empirical orthogonal functions. *Monthly Weather Review*, 110, 699–706.
- O'Lenic, E. A., & Livezey, R. E. (1988). Practical considerations in the use of rotated principal component analysis (RPCA) in diagnostic studies of upper-air height fields. *Monthly Weather Review*, 116, 1682–1689.
- Raible, C. C., Lehner, F., González-Rouco, J. F., & Fernández-Donado, L. (2014). Changing correlation structures of the Northern Hemisphere atmospheric circulation from 1000 to 2100 AD. *Climate of the Past*, 10, 537–550. <https://doi.org/10.5194/cp-10-537-2014>
- Richman, M. B. (1986). Rotation of principal components. *Journal of Climatology*, 6, 293–335.
- Richman, M. B. (1993). Comments on “The effect of domain shape on principal component analyses”. *International Journal of Climatology*, 13, 203–218.
- Richman, M. B., & Lamb, P. J. (1985). Climatic pattern analysis of three- and seven-day summer rainfall in the Central United States: Some methodological considerations and a regionalization. *Journal of Climate and Applied Meteorology*, 24, 1325–1343.
- Rogers, J. C. (1981). Spatial variability of seasonal sea level pressure and 500 mb height anomalies. *Monthly Weather Review*, 109, 2093–2106.
- Skeie, P. (2000). Meridional flow variability over the Nordic seas in the Arctic oscillation framework. *Geophysical Research Letters*, 27, 2569–2572. <https://doi.org/10.1029/2000GL011529>
- Smoliak, B. V., & Wallace, J. M. (2015). On the leading patterns of Northern Hemisphere sea level pressure variability. *Journal of the Atmospheric Sciences*, 72, 3469–3486. <https://doi.org/10.1175/JAS-D-14-0371.1>
- Spensberger, C., Reeder, M. J., Spengler, T., & Patterson, M. (2020). The connection between the Southern Annular Mode and a feature-based perspective on Southern Hemisphere midlatitude winter variability. *Journal of Climate*, 33, 115–129. <https://doi.org/10.1175/JCLI-D-19-9224.1>
- Thompson, D. W. J., & Wallace, J. M. (1998). The Arctic oscillation signature in the wintertime geopotential height and temperature fields. *Geophysical Research Letters*, 25, 1297–1300. <https://doi.org/10.1029/98GL00950>
- Tremblay, L.-B. (2001). Can we consider the Arctic oscillation independently from the Barents oscillation? *Geophysical Research Letters*, 28, 4227–4230. <https://doi.org/10.1029/2001GL013740>
- Walker, G. (1933). Seasonal weather and its prediction. *Nature*, 132, 805–808.
- Walker, G. T., & Bliss, E. W. (1932). World weather V. *Memoirs of the Royal Meteorological Society*, 4, 53–84.
- Wallace, J. M., & Gutzler, D. S. (1981). Teleconnections in the geopotential height field during the Northern Hemisphere winter. *Monthly Weather Review*, 109, 784–812.
- Woolings, T., Hoskins, B., Blackburn, M., & Berrisford, P. (2008). A new Rossby wave-breaking interpretation of the North Atlantic oscillation. *Journal of the Atmospheric Sciences*, 65, 609–626. <https://doi.org/10.1175/2007JAS2347.1>
- Wulff, C. O., Greatbatch, R. J., Domeisen, D. I. V., Gollan, G., & Hansen, F. (2017). Tropical forcing of the summer East Atlantic pattern. *Geophysical Research Letters*, 44, 11166–11173. <https://doi.org/10.1002/2017GL075493>
- Ye, S.-W., Yi, D.-W., Sung, M.-K., & Kim, Y. H. (2018). An eastward shift of the North Pacific oscillation after the mid-1990s and its relationship with ENSO. *Geophysical Research Letters*, 45, 6654–6660. <https://doi.org/10.1029/2018GL078671>
- Zhang, W., Li, J., & Zhao, X. (2010). Sea surface temperature cooling mode in the Pacific cold tongue. *Journal of Geophysical Research*, 115, C12042. <https://doi.org/10.1029/2010JC006501>
- Zwiers, F. W., & von Storch, H. (2004). On the role of statistics in climate research. *International Journal of Climatology*, 24, 665–680. <https://doi.org/10.1002/joc.1027>